Oral Presentation

The 7th TSME International Conference on Mechanical Engineering
13-16 December 2016

TSME ICOME 2016
Mechanical Engineering Innovation for Green Society

DRC0002

Stabilizing Active Vibration Control of Machining Processes Based on Lyapunov-Krasovskii Functionals for Time-Delay Systems

Prapon Ruttanatri*, Matthew O.T. Cole and Radom Pongvuthithum

Department of Mechanical Engineering, Chiang Mai University,
239 Huay Gaew Rd. Suthep, Muang, Chiang Mai 50200
* Corresponding Author: praponruttanatri@hotmail.co.th, Telephone 66 53 94 4146, Fax 66 53 94 4145

Abstract

This paper considers the problem of feedback controller design for active control of regenerative vibration in machining processes. A magnetic bearing supported milling machine spindle is considered in case study. In order to predict vibrational stability, a dynamic model of spindle flexibility is considered that accounts for the deflection of the tool due to cutting forces. As the tool deflection during tooth-pass affects the cutting force during the next tooth-pass, a complete model for tool-workpiece interaction takes the form of a time-delay system. In this paper, a stability analysis based on LMI conditions derived from a Lyapunov-Krasovskii functional is considered in order to predict boundaries for stable cutting and synthesize state-feedback controllers to increase parametric regions for stable cutting. A finite element model of the spindle-tool structure is adopted. However, for numerical efficiency, a reduced order model of the machine structure is used for the synthesis. A robust controller design approach based on an augmented plant model is introduced to deal with issues of model uncertainty. Comparative results for optimized state feedback control versus position-based PD feedback are presented. Numerical simulations confirm that the proposed design gives significant improvements in vibration and allow increased metal removal rates with stable cutting.

Keywords: Vibration control, Machining, Time-delay systems, Active magnetic bearing, Stability.

1. Introduction

It is well-known that the vibrational dynamics of many cutting processes involve a time-delayed feedback effect which can lead to instability known as "*chatter*" [1-9]. Chatter involves self-excitation of flexible structure vibration within the machine and/or workpiece and this places practical limit on material removal rate. For a machine spindle supported by magnetic bearings, there is the potential to apply advanced control methods in order to avoid chatter [10], [11].

Controller design approaches for time-delay systems may involve a set of LMIs (Linear Matrix Inequalities) derived from a suitably chosen Lyapunov-Krasovskii functional (LKF) [12], [13]. There has been limited research on applying these techniques in real machining processes.

In this paper, we aim to develop a methodology for designing active vibration controllers for suppressing chatter in machining process. The considered system consists of a machine tool spindle supported by an active magnetic bearing (AMB) which can apply control forces to the spindle based on feedback of measured position/velocity variables. A standard controller using PD feedback of measured spindle position within the AMB is implemented to obtain a stable system when not cutting [14]. The traditional frequency response analysis methods are used to obtain stability lobe diagrams for this base-line system [3]. These diagrams indicate the maximum stable cutting depth/feed-rate. Predictions of stability regions are also obtained by LMI optimization [15] based on LKF analysis and the results compared.

To improve stability limits, a robust state feedback controller design approach is introduced and applied to the described system model. This approach involves introducing an augmented system model that can ensure closed loop stability in the presence of model uncertainty via application of the small gain theorem [16]. Simulation results are shown for further validation of the approach.

2. System Modeling

2.1 Finite Element Model for Spindle Dynamics

Typically, a milling machine spindle is supported by a set of ball bearings. An actively controlled spindle can be realized by replacing one conventional bearing by a radial AMB as shown in Fig. 1.

To apply finite element methods (FEM) [17] the spindle can be considered as an assembly of n elements. Application of Galerkin's method leads to an element equation in the form:

$$\mathbf{M}^{(i)}\ddot{\xi}^{(i)} + \mathbf{K}^{(i)}\xi^{(i)} = f_R{}^{(i)} \qquad (1)$$

where $\mathbf{M}^{(i)}$ and $\mathbf{K}^{(i)}$ are the symmetric mass and stiffness matrices for the i^{th} element.

To limit model complexity in the current study, we neglect the gyroscopic effect which would cause a cross-coupling between transverse planes. Hence, the system dynamics may be described by a 2D model. By combining equations for each element (Eq. (1)) together, the system equation of motion for a spindle is obtained in the form

DRC0002

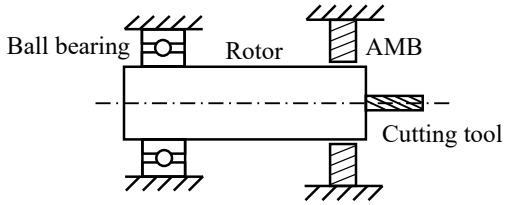

Fig. 1 Machine spindle with a radial AMB

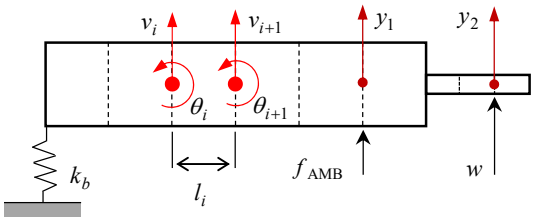

Fig. 2 Spindle elements model

$$\mathbf{M}\ddot{\xi}+\mathbf{C}\dot{\xi}+\mathbf{K}\xi=f_{ext}. \tag{2}$$

Where $\mathbf{C}$ is a damping matrix, for which it is convenient to assume the proportional form: $\mathbf{C}=\alpha\mathbf{M}+\beta\mathbf{K}$ when, α and β are constants. The vector $\xi=\{v_1 \quad \theta_1 \quad \ldots\ldots \quad v_{n+1} \quad \theta_{n+1}\}^T$ contains generalized coordinates with v_i and θ_i being the linear and rotational displacements at the i^{th} node. The effect of passive bearing forces are accounted for within the matrix $\mathbf{K}$ by additional stiffness terms.

Referring to Fig. 2, the external force vector f_{ext} includes the cutting force, w, and magnetic bearing force, f_{AMB}. Thus, the external forces can be described as follows:

$$\begin{aligned} f_{ext} &= \mathbf{E}_u f_{\text{AMB}} + \mathbf{E}_w w \\ &= \mathbf{E}_u (f_{neg} + u_{PD} + u) + \mathbf{E}_w w \end{aligned} \tag{3}$$

where the matrices $\mathbf{E}_u$ and $\mathbf{E}_w$ are chosen to allocate the forces at the appropriated nodes. Note the AMB force can be considered as having three components due to negative stiffness f_{neg}, PD feedback of local position measurements u_{PD}, and additional control force u, which will be determined by an optimized control design later.

The negative stiffness force depends on the displacement at the magnetic bearing so that, $\mathbf{E}_u f_{neg}=-\mathbf{K}_s\xi$. Therefore, the system equation of motion can be written in the form:

$$\mathbf{M}\ddot{\xi}+\mathbf{C}\dot{\xi}+(\mathbf{K}+\mathbf{K}_s)\xi=\mathbf{E}_u u_{PD}+\mathbf{E}_u u+\mathbf{E}_w w. \tag{4}$$

Consequently, a state-space description is given by

$$\dot{v}_s=\mathbf{A}_s v_s+\mathbf{B}_{su}u_{PD}+\mathbf{B}_{su}u+\mathbf{B}_{sw}w \tag{5}$$

where, $\mathbf{A}_s=\begin{bmatrix}\mathbf{0} & \mathbf{I}\\ -\mathbf{M}^{-1}(\mathbf{K}+\mathbf{K}_s) & -\mathbf{M}^{-1}\mathbf{C}\end{bmatrix}$, $\mathbf{B}_{su}=\begin{bmatrix}\mathbf{0}\\ \mathbf{M}^{-1}\mathbf{E}_u\end{bmatrix}$ and $\mathbf{B}_{sw}=\begin{bmatrix}\mathbf{0}\\ \mathbf{M}^{-1}\mathbf{E}_w\end{bmatrix}$. The state variable is $v_s=\left\{\xi^T \quad \dot{\xi}^T\right\}^T$. In Laplace domain, the PD controller is defined with a filtered derivative as

$$U_{PD}(s)=\left(-K_P-\frac{K_D s}{\tilde{\tau}s+1}\right)Y_1(s)$$

where y_1 is the measured displacement at AMB which can be expressed as $y_1=\mathbf{C}_1 v_s$. Therefore, the state-space form of PD controller takes the form:

$$\begin{aligned} \dot{v}_c &= \mathbf{A}_c v_c + \mathbf{B}_c \mathbf{C}_1 v_s \\ u_{PD} &= \mathbf{C}_c v_c + \mathbf{D}_c \mathbf{C}_1 v_s \end{aligned} \tag{6}$$

Combining Eq. (5) and (6), the system with PD controller can be written by the form:

$$\dot{v}=\hat{\mathbf{A}}v+\hat{\mathbf{B}}_u u+\hat{\mathbf{B}}_w w \tag{7}$$

where $\hat{\mathbf{A}}=\begin{bmatrix}\mathbf{A}_s+\mathbf{B}_{su}\mathbf{D}_c\mathbf{C}_1 & \mathbf{B}_{su}\mathbf{C}_c\\ \mathbf{B}_c\mathbf{C}_1 & \mathbf{A}_c\end{bmatrix}$, $\hat{\mathbf{B}}_u=\begin{bmatrix}\mathbf{B}_{su}\\ \mathbf{0}\end{bmatrix}$, $\hat{\mathbf{B}}_w=\begin{bmatrix}\mathbf{B}_{sw}\\ \mathbf{0}\end{bmatrix}$ and the state vector is $v=\begin{Bmatrix}v_s^T & v_c^T\end{Bmatrix}^T$. System outputs may be defined and expressed in terms of state variables as $y_2=\hat{\mathbf{C}}_2 v$ and $y=\hat{\mathbf{C}}v$ where y_2 is the deflection of the tool at the cutting location and y is the full set of measurement variables available for control feedback.

2.2 Model Order Reduction

To simplify the synthesis and realization of a state feedback controller, the approach here is to find the minimum-order model that retains structural modes that are critical to vibrational stability. For a typical rotor geometry shown in Fig. 2 the low frequency dynamics combine the rigid body motion of the rotor within the AMB with a higher frequency mode associated with flexibility of the cutting tool. To capture these dynamics within a low order model, the high-order model in Eq. (7) is first transformed into a Jordan canonical form [16]. Eliminating the modal states associated with other higher frequency modes leads to a fourth order system:

$$\begin{aligned} \dot{x} &= \mathbf{A}x+\mathbf{B}_u u+\mathbf{B}_w w \\ y_2 &= \mathbf{C}_2 x\,. \end{aligned} \tag{8}$$

This linear dynamic model must be combined with a model for tool-workpiece interaction that

defines how y_2 depends on w. This model will be described in the next section.

2.3 Tool – Workpiece Interaction

The established 1-D model for the cutting force in milling is [3]:

$$w(t) = bK_{cut}N_t^*\left(h_m(t) - y_2(t) + y_2(t-\tau)\right) \qquad (9)$$

Here, K_{cut} is the material force coefficient for cutting, b is axial depth of cut and N_t^* is a factor that relates to the average number of operating teeth (which depends on the radial immersion and the total number of teeth). The basic assumption here is that the force generated is proportional to the instantaneous rate of material removal. The variable $h_m(t)$ is the chip thickness for cutting with zero vibration. The net force $w(t)$ depends on the current chip thickness. This depends on current tool position and the location of the surface of the workpiece, which depends on the previous cut. This concept is illustrated in Fig. 3. Thus, a time-delay term $y_2(t-\tau)$ arises, where τ is the time interval between the current and previous tooth-pass. Therefore, $\tau = 2\pi / N_t\Omega$ where N_t is the number of teeth and Ω is the rotational speed of the spindle.

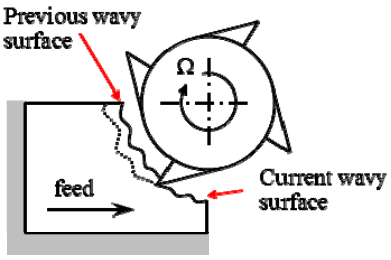

Fig. 3 Tool-workpiece interaction conceptual model

Table. 1 Spindle model properties for FEM

Spindle diameter	30	mm
Spindle length	200	mm
n -spindle	20	–
Cutting tool diameter	5	mm
Cutting tool length	40	mm
n -cutting tool	5	–
Density	7.89	kg/m^3
Young's modulus of elasticity	205	GPa

2.4 System Parameters for Case study

For further investigations, a system model is defined based on the spindle configuration shown in Fig. 2. A model is derived using the parameter values in Table 1. Fig. 4 shows a comparison of the frequency response of G_{y_2w} for the full-order model Eq. (7) and the fourth-order reduced model Eq. (8). It can be seen that the reduced order model matches well over the low frequency range covering the first two natural modes of vibration ($\omega_{n1} = 3080.59$ rad/sec and $\omega_{n2} = 13937.76$ rad/sec) while large differences exist at high frequencies corresponding to eliminated modes. The second mode is associated with tool flexure and will be referred to as the tool-tip mode. For a real system, damping of high frequency modes may be somewhat higher due to effects from material internal damping, which have not been included in the model.

Fig. 5 shows how the frequency response of the reduced-order model varies as the PD controller derivative gain is changed. It can be observed that *the PD control has little influence* over the behavior of the high frequency mode 2. This will have important implications for the effectiveness of PD control in preventing chatter instability.

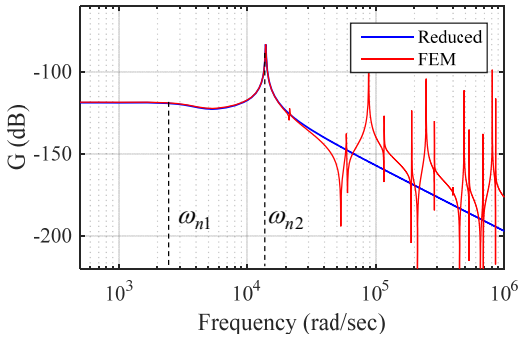

Fig. 4 Spindle frequency response G_{y_2w} with local PD control of AMB: $K_P = 4000$ N/m, $K_D = 250$ Ns/m

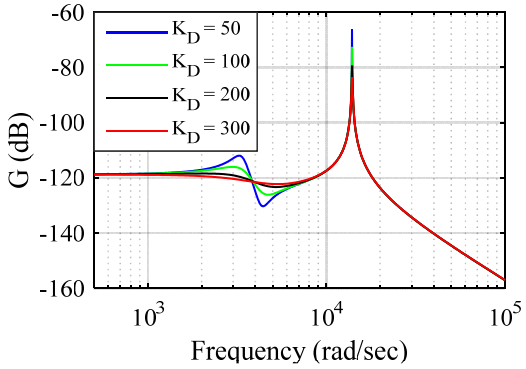

Fig. 5 Spindle frequency response with PD control: derivative gain varied $K_D = 50 \rightarrow 300$ Ns/m

3. Stability Boundaries for Milling

The conventional approach to predict parametric boundaries for vibrational stability in machining is based on a frequency response analysis [3]. This method can be used to produce stability lobe diagrams which can then be used to set machine operating parameters. Considering Eq. (8) with the control force set to zero, the transfer function from cutting force to

the cutting tool displacement (SISO) can be defined $G(s)=\mathbf{C}_2(s\mathbf{I}-\mathbf{A})^{-1}\mathbf{B}_w$ so that

$$Y_2(s)=G(s)W(s) \tag{10}$$

Similarly, Eq. (9) can be converted to the Laplace domain:

$$W(s)=bK_{cut}k_t^*\left(H_m(s)-(1-e^{-\tau s})Y_2(s)\right).$$

Therefore, the overall transfer function of the system, including cutting force dynamics, is

$$\frac{Y_2(s)}{H_m(s)}=\frac{bK_{cut}k_t^*G(s)}{1+bK_{cut}k_t^*G(s)(1-e^{-\tau s})} \tag{11}$$

The characteristic equation is

$$1+b_K G(s)(1-e^{-\tau s})=0 \tag{12}$$

where the constant parameters are combined within a single 'depth of cut' parameter $b_K=bK_{cut}k_t^*$.

To solve for a limit cycle vibratory solution we seek solutions to Eq. (12) with $s=j\omega_c$ where ω_c is the frequency of chatter. The equations for real and imaginary parts are

I) $1+b_K\,\mathrm{Re}\left(G(j\omega_c)(1-e^{-\tau j\omega_c})\right)=0$,

II) $\mathrm{Im}\left(G(j\omega_c)(1-e^{-\tau j\omega_c})\right)=0$,

The second equation implies

$$\tau\omega_c=\pi+2\angle G(j\omega_c)+2\pi N_c$$

where $N_c=0,\ 1,\ 2,\ \ldots.$ is the cycle number for the time-delay. Then, from the first equation, the stability limit (maximum) value for the depth of cut parameter is

$$b_{K,\max}=\frac{-1}{2\,\mathrm{Re}\left(G(j\omega_c)\right)}$$

For each value of chatter frequency ω_c there are multiple solutions for the time delay:

$$\tau=\frac{2\angle G(j\omega_c)}{\omega_c}+\frac{\pi}{\omega_c}+\frac{2\pi N_c}{\omega_c}$$

Then, from $\tau=2\pi/N_t\Omega$, the rotational frequency corresponding to the stability limit given by $b_{K,\max}$ is

$$\Omega=N_t\omega_c\left(\frac{\angle G(j\omega_c)}{\pi}+\frac{1}{2}+N_c\right)^{-1}$$

where $N_c=0,\ 1,\ 2,\ \ldots.$

The solutions to Eq. (12) allow us to plot the stability limit in terms of the depth of cut parameter, $b_{K,\max}$ versus spindle speed, Ω (rad/sec). The stability lobe diagram is shown for the test case under consideration in Fig. 6. The region for stable cutting operation is below all the lobes generated with different values for N_c. The stability limit for operation at any rotational speed is also indicated in Fig. 6 and is approximately $b_{K,LB}\approx 1.183\times10^4$ N/m.

4. Robust Controller Design Formulation

To guarantee that the controller from Eq. (8) can be applied in practice to a real system, the robust control approach [10], [11] is applied to account for existent model error/uncertainty.

The augmented system/plant for the robust control approach is shown in Fig. 7. A weighting function, W_r, is a transfer function chosen such that $|W_r|$ exceeds the multiplicative uncertainty [16] for the system frequency response. According to the small gain theorem [15], if the closed loop system model T_{ud} (from d to u) satisfies

$$\left\|T_{\tilde{u}\tilde{d}}\right\|_\infty=\left\|W_rT_{ud}\right\|_\infty<1, \tag{13}$$

then, the closed loop system will always be stable. The augmented state vector of the closed loop system can be obtained by combining the system state x and weighting function state x_r in the form: $\tilde{x}=\begin{Bmatrix}x^T & x_r^T\end{Bmatrix}^T$.

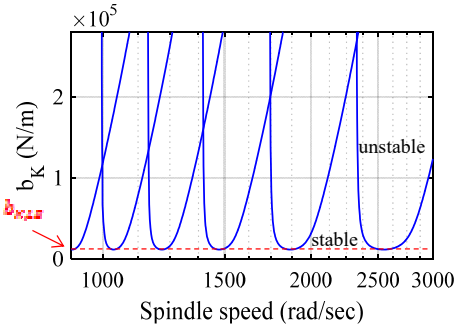

Fig. 6 Stability lobe diagram for test case with PD control for $K_D=250$ Ns/m

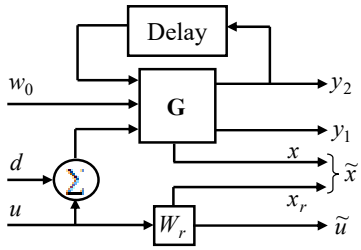

Fig. 7 The spindle model with weighting function, W_r

For a good control performance under cutting, we require that the system is stable for an increased value of b_K compared with the basic PD control approach. In general, this would allow higher metal removal

rates to be achieved. The weighting function in a state-space form is defined by

$$\begin{aligned} \dot{x}_r &= \mathbf{A}_r x_r + \mathbf{B}_r u \\ \tilde{u} &= \mathbf{C}_r x_r + \mathbf{D}_r u \,. \end{aligned} \tag{14}$$

Then, the augmented system can be determined from Eq. (8) and Eq. (14) by

$$\begin{aligned} \dot{\tilde{x}} &= \tilde{\mathbf{A}}\tilde{x} + \tilde{\mathbf{B}}_u u + \tilde{\mathbf{B}}_d d + \tilde{\mathbf{B}}_w w \\ y_2 &= \tilde{\mathbf{C}}_2 \tilde{x} \\ \tilde{u} &= \tilde{\mathbf{C}}_r \tilde{x} + \tilde{\mathbf{D}}_r u \end{aligned} \tag{15}$$

where $\tilde{\mathbf{A}} = \begin{bmatrix} \mathbf{A} & \mathbf{0} \\ \mathbf{0} & \mathbf{A}_r \end{bmatrix}$, $\tilde{\mathbf{B}}_u = \begin{bmatrix} \mathbf{B}_u \\ \mathbf{B}_r \end{bmatrix}$, $\tilde{\mathbf{B}}_d = \begin{bmatrix} \mathbf{B}_u \\ \mathbf{0} \end{bmatrix}$, $\tilde{\mathbf{B}}_w = \begin{bmatrix} \mathbf{B}_w \\ \mathbf{0} \end{bmatrix}$, $\tilde{\mathbf{C}}_2 = \begin{bmatrix} \mathbf{C}_2 & \mathbf{0} \end{bmatrix}$, $\tilde{\mathbf{C}}_r = \begin{bmatrix} \mathbf{0} & \mathbf{C}_r \end{bmatrix}$, $\tilde{\mathbf{D}}_r = \mathbf{D}_r$.

The time-delay system is modified by putting the cutting force model, Eq. (9), into Eq. (15) as follows

$$\begin{aligned} \dot{\tilde{x}} &= \tilde{\mathbf{A}}_0 \tilde{x} + \tilde{\mathbf{A}}_1 \tilde{x}(t-\tau) + \tilde{\mathbf{B}}_u u + \tilde{\mathbf{B}}_d d + \tilde{\mathbf{B}}_w w_0 \\ y_2 &= \tilde{\mathbf{C}}_2 \tilde{x} \\ \tilde{u} &= \tilde{\mathbf{C}}_r \tilde{x} + \tilde{\mathbf{D}}_r u \end{aligned} \tag{16}$$

where $\tilde{\mathbf{A}}_0 = \tilde{\mathbf{A}} - \tilde{\mathbf{B}}_w b_K \tilde{\mathbf{C}}_2$, $\tilde{\mathbf{A}}_1 = \tilde{\mathbf{B}}_w b_K \tilde{\mathbf{C}}_2$ and the zero vibration cutting force is $w_0 = b_K h_m(t)$.

In this study a linear state feedback control law is considered in the form

$$u(t) = \mathbf{K}\tilde{x}(t) \,. \tag{17}$$

where an optimized state feedback gain $\mathbf{K}$ is to be determined. Note that this controller could be implemented only if the number and type of vibration measurements is sufficient to give full state information. Nonetheless it is an important test case to study. To satisfy the H_∞ norm–bound criterion Eq. (13). The following equivalent condition may be considered

$$\|\tilde{u}\|_{L_2} \le \|d\|_{L_2} \,, \ \forall \quad d \in L_2[0,\infty) \,. \tag{18}$$

For the robust stability analysis, we may set the exogenous component of the cutting force to be zero, $w_0 = 0$. The equation (15) is satisfied if there exists a Lyapunov-Krasovskii functional (LKF) $V(\tilde{x},t)$ such that

$$\dot{V}(\tilde{x},t) + \tilde{u}^T\tilde{u} - d^T d \le 0 \,. \tag{19}$$

The LKF $V(\tilde{x},t)$ is chosen as [12]

$$V(\tilde{x},t) = \tilde{x}^T \mathbf{P}\tilde{x} + \int_{t-\tau}^{t} \tilde{x}^T(\alpha)\mathbf{Q}\tilde{x}(\alpha)d\alpha \tag{20}$$

with $\mathbf{P} = \mathbf{P}^T > 0$, $\mathbf{Q} = \mathbf{Q}^T > 0$ and $\tau > 0$ is the time delay parameter. Then, Eq. (19) has the quadratic form,

$$\xi^T \mathbf{\Phi} \xi \le 0 \,,$$

where, $\xi = \begin{bmatrix} \tilde{x}^T(t) & \tilde{x}^T(t-\tau) & d \end{bmatrix}^T$. This inequality will always hold if the matrix $\mathbf{\Phi}$ is negative definite. To obtain an equivalent condition in LMI form the standard Schur complement transformations [15] may be applied to yield:

$$\mathbf{\Psi} = \begin{bmatrix} \phi_{11} & \phi_{12} & \phi_{13} & \phi_{14} \\ & \phi_{22} & \phi_{23} & \phi_{24} \\ & & \phi_{33} & \phi_{34} \\ \text{sym} & & & \phi_{44} \end{bmatrix} < 0 \,, \tag{21}$$

where,

$$\begin{aligned} &\phi_{11} = \mathbf{P}\left(\tilde{\mathbf{A}}_0 + \tilde{\mathbf{B}}_u^T \mathbf{K}\right) + \left(\tilde{\mathbf{A}}_0 + \tilde{\mathbf{B}}_u^T \mathbf{K}\right)^T \mathbf{P} + \mathbf{Q} \,, \\ &\phi_{12} = \mathbf{P}\tilde{\mathbf{A}}_1 \,, \ \phi_{13} = \mathbf{P}\tilde{\mathbf{B}}_d \,, \phi_{14} = \tilde{\mathbf{C}}_r^T + \mathbf{K}^T \tilde{\mathbf{D}}_r^T \,, \\ &\phi_{22} = -\mathbf{Q} \,, \ \phi_{23} = \phi_{24} = \phi_{34} = \mathbf{0} \,, \\ &\phi_{33} = -\mathbf{I} \,, \ \phi_{44} = -\mathbf{I} \,. \end{aligned}$$

If there is a solution to the LMI Eq. (21), then the time-delay system in Eq. (16) is stable and the H_∞ norm from d to $\tilde{u}$ less than 1.

The LMI in Eq. (21) will have additional terms that are bilinear and involve $\mathbf{P}$, $\mathbf{K}$. In order to recover an LMI that can be solved for $\mathbf{K}$ in addition to the other free variables, we can apply a congruency transformation with the matrix

$$\mathbf{\Theta} = \text{diag}\left[\mathbf{P}^{-1} \quad \mathbf{P}^{-1} \quad \mathbf{I} \quad \mathbf{I}\right]$$

followed by a substitution of variables $\mathbf{L} = \mathbf{P}^{-1}$, $\mathbf{S} = \mathbf{L}^T\mathbf{Q}\mathbf{L}$, $\tilde{\mathbf{K}} = \mathbf{K}\mathbf{L}$. This leads to the following LMI feasibility problem.

If there exist positive definite matrices, $\mathbf{L} > 0$, $\mathbf{S} > 0$ and matrix $\tilde{\mathbf{K}}$ such that the following LMI holds:

$$\mathbf{\Xi} = \begin{bmatrix} \theta_{11} & \theta_{12} & \theta_{13} & \theta_{14} \\ & \theta_{22} & \theta_{23} & \theta_{24} \\ & & \theta_{33} & \theta_{34} \\ \text{sym} & & & \theta_{44} \end{bmatrix} < 0 \tag{22}$$

where

$$\begin{aligned} &\theta_{11} = \tilde{\mathbf{A}}_0\mathbf{L} + \mathbf{L}\tilde{\mathbf{A}}_0^T + \tilde{\mathbf{B}}_u\tilde{\mathbf{K}} + \tilde{\mathbf{K}}^T\tilde{\mathbf{B}}_u^T + \mathbf{S} \\ &\theta_{12} = \tilde{\mathbf{A}}_1\mathbf{L} \,, \ \theta_{13} = \tilde{\mathbf{B}}_d \,, \ \theta_{14} = \mathbf{L}\tilde{\mathbf{C}}_r^T + \tilde{\mathbf{K}}^T\tilde{\mathbf{D}}_r^T \\ &\theta_{22} = -\mathbf{S} \,, \ \theta_{33} = -\mathbf{I} \,, \ \theta_{44} = -\mathbf{I} \\ &\theta_{23} = \theta_{24} = \theta_{34} = \mathbf{0} \,. \end{aligned}$$

Then, the time-delay system in Eq. (16) with control law, $u(t) = \widetilde{\mathbf{K}}\mathbf{L}^{-1}\widetilde{x}(t)$ is stable and the H_∞ norm from d to $\widetilde{u}$ less than 1.

Note that, we can also calculate the time-delay system stability region by using the same LKF but without the H_∞ norm-bound, giving an LMI in $\mathbf{P}$ and $\mathbf{Q}$:

$$\mathbf{H}_0 = \begin{bmatrix} \mathbf{P}\widetilde{\mathbf{A}}_0 + \widetilde{\mathbf{A}}_0^T\mathbf{P} + \mathbf{Q} & \mathbf{P}\widetilde{\mathbf{A}}_1 \\ \widetilde{\mathbf{A}}_1^T\mathbf{P} & -\mathbf{Q} \end{bmatrix} < 0 \qquad (23)$$

If this problem is feasible, which can be checked using a standard LMI solver (e.g. "*feasp*" in Matlab), then the system is stable. To find the maximum depth of cut, $b_{K,\max}$, we can repeatedly solve the feasibility problem with iteration over b_K e.g. using a bisection algorithm.

5 Simulation Results

The feedback control synthesis method is applied to the test case spindle model with properties listed in Table 1. The initial system for synthesis involves the PD controlled case (results are shown in Fig. 4-6) with gains $K_P = 4000$ N/m, $K_D = 250$ Ns/m.

The key performance parameter that relates to the maximum metal removal rate with stable cutting is $b_{K,\max}$. We adopt the weighting function W_r as a general second order transfer function

$$W_r = K_w \frac{s^2 + 2\zeta_1\omega_1 s + \omega_1^2}{s^2 + 2\zeta_2\omega_2 s + \omega_2^2}.$$

Where, $\zeta_1 = \zeta_2 = 1$, $\omega_1 = 9{,}000$ rad/sec, $\omega_2 = 20{,}000$ rad/sec. To evaluate the control synthesis approach, we focus on two key parameters in the system model, which are the depth of cut parameter, b_K, and the weighting function scaling K_w which is a positive scalar and can be considered as a relative measure of the plant uncertainty, i.e. an indicator of controller robustness.

For a given values for the depth of cut parameter b_K we calculate a control solution for the maximum possible value of K_w. This is achieved by using a bisection algorithm to select K_w and then using a standard LMI solver (Matlab command "*feasp*") to solve Eq. (22). The values of $K_{w,\max}$ are quite similar for the range of b_K used ($b_K = 1\times10^4 \rightarrow 2\times10^4$ N/m). Note that the value of $b_{K,\max}$ with PD control alone is $b_{K,\max} \approx 1.183\times10^4$ N/m. Results will be shown for two different cases of optimized state feedback control which correspond to values of $b_K = 1.5\times10^4$ N/m and $b_K = 2.0\times10^4$ N/m used in the synthesis LMI. The corresponding value of $K_{w,\max}$ are $K_{w,\max} = 2.0765$ and $K_{w,\max} = 2.0807$ respectively.

In summary the results may be presented for three different controller cases:

C1: PD controller only, $u = 0$

C2: PD + state feedback control ($b_K = 1.5\times10^4$ N/m)

C3: PD + state feedback control ($b_K = 2.0\times10^4$ N/m)

Note that for C2 and C3 the total control force, u_{total}, is a summation of the PD control force component, u_{PD}, and the state feedback control force component, u. Thus $u_{total} = u_{PD} + u$ in accordance with Eq. (3).

The state feedback gain results for C2 and C3 are shown in Table 2.

Table. 2 Synthesis results: State feedback gains

C2, $\mathbf{K}$ =					
$[1.28$	-0.84	-0.00028	0.00011	0.020	$287.9]\times10^6$
C3, $\mathbf{K}$ =					
$[1.79$	-2.68	-0.00237	0.00086	0.012	$186.7]\times10^6$

Table. 3 The maximum stable depth of cut parameter

Controller	$b_{K,\max}$ (N/m)
C1	1.18×10^4
C2	1.41×10^5
C3	3.19×10^5

The robustness properties for the controlled system can be seen in Fig. 8, which shows the complementary sensitivity function, T_{ud}. The frequency response (singular values) of the inverse of the weighting function W_r^{-1} exceed the maximum singular value of T_{ud}, as expected by Eq. (13).

The closed loop frequency response of the system with the three controller cases are shown in Fig. 9. The cases with state feedback control show significant decreased in the resonance due to the tool-tip vibration mode (around 14000 rad/s). This resonance has the dominant effect on the maximum depth of cut parameter $b_{K,\max}$. The stability limits, in terms of b_K are shown for the three cases in Table 3.

The larger parametric regions for stable cutting with state feedback control C2 and C3 against to the system with a PD controller only C1 can also be seen in the stability lobe diagram plot in Fig. 10.

Note that solving the LMI feasibility problem Eq. (23) for the controlled system gives a tighter bound on the actual stability region than the synthesis LMI. It can be observed that LMI condition gives a tight lower bound on the stability limit $b_{K,\max}$ over all values of spindle speed Ω (shown only for case C1). However,

DRC0002

it must also be concluded that the LMI conditions derived from the chosen LKF cannot capture the detailed structure of the stability lobe diagram.

Time-step simulations where performed using Matlab Simulink models that combine a standard cutting process model for milling [3] with the state space descriptions of the closed loop system. The operating points (a, b, c, d) for simulation of controllers C1 and C2 were chosen based on the stability lobe diagram, as shown in Fig. 11. The corresponding spindle speed is $\Omega = 1325$ rad/sec.

The cutting simulation results in terms of the tool tip vibration, y_2, and the total control force, u_{total}, can be seen in Figs 12 and 13 for controllers C1 and C2 respectively. It can be seen that for operation within the stability region, ($b_K = 7\times10^4$ N/m for C1 and $b_K = 15\times10^4$ N/m for C2) the amplitude of vibration converges but for the instability region, ($b_K = 9\times10^4$ N/m for C1 and $b_K = 17\times10^4$ for C2) the amplitude of vibration diverges.

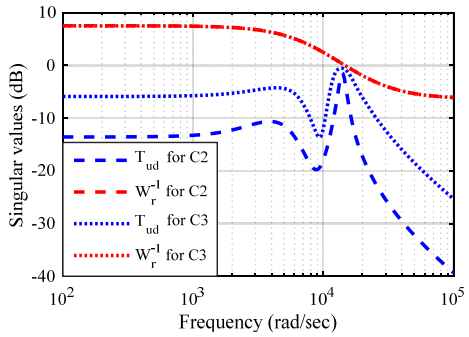

Fig. 8 Robust stability

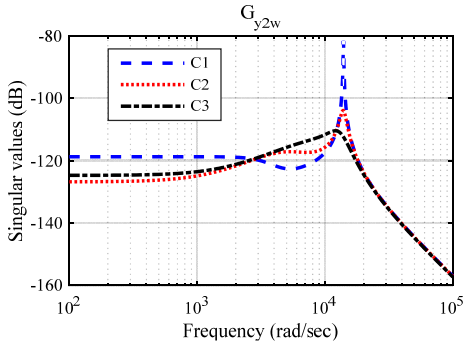

Fig. 9 Spindle frequency response

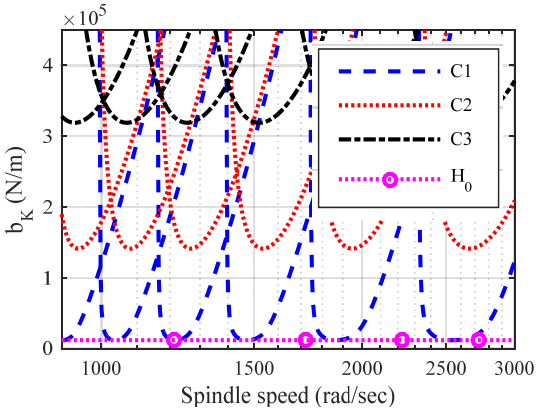

Fig. 10 Stability lobe diagram

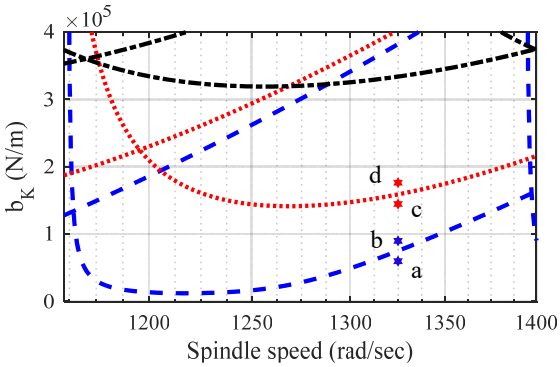

Fig. 11 The operating points chosen for simulation: stable and unstable regions for C1 and C2 with spindle speed $\Omega = 1325$ rad/sec

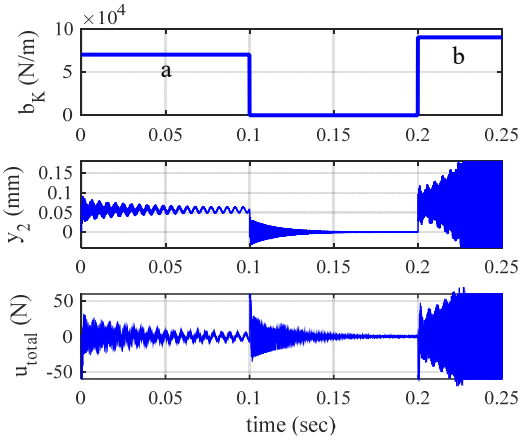

Fig. 12 Cutting simulation results for C1 with spindle speed $\Omega = 1325$ rad/sec

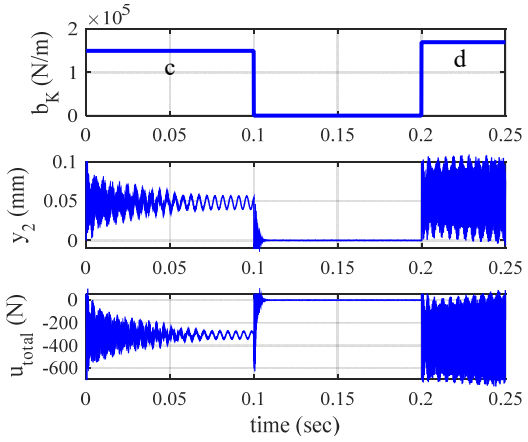

Fig. 13 Cutting simulation results for C2 with spindle speed $\Omega = 1325$ rad/sec

6. Conclusions

Vibration of a milling machine spindle system with AMBs can be controlled using a parallel connection of a PD controller and robust state feedback controller in order to improve stability of vibration during cutting.

It has been shown that local PD control has limited influence for preventing vibrational instability due to spindle/tool flexibility. Combining an LKF-based stability criterion and the weighted H_∞ norm–bound criterion allows a synthesis of robust state feedback controllers to improve stability limits.

The simulation results of cutting process for stable and unstable cutting situations confirm the effectiveness of the control approach. Extending the approach for implementation on an experimental system will be the focus of further work.

7. References

[1] S. A. Tobias and A.H. Burton, *Machine-tool vibration*, London: Blackie, 1965.

[2] J. Tlusty, "Dynamics of High-Speed Milling," *Journal of Engineering for Industry,* vol. 108, p. 59, 1986.

[3] T. L. Schmitz, K. S. Smith, *Machining Dynamics, Frequency Response to Improved Productivity*, Springer Science+Business Media, LLC, 2009.

[4] Y, Altintas; G, Stepan; D, Merdol; Z, Dombovari, "Chatter stability of milling in frequency and discreate time domain," *CRIP Journal of Manufacturing Science and Technology,* vol. 1 no.1, 2008, pp. 35-44.

[5] T. L. Schmitz, K. S. Smith, *Machining Dynamics*, USA: Springer, 2009.

[6] An-Chen Lee, Chia-Shang Liu, Shiuh-Tarng Chiang, "Analysis of chatter vibration in a cutter-workpiece system," *International Journal of Machine Tools and Manufacture,* vol. 31, no. 2, pp. 221-234, 1991.

[7] S. Smith and J. Tlusty, "An Overview of Modeling and Simulation of the Milling Process," *Journal of Engineering for Industry,* vol. 113, p. 169, 1991.

[8] H. Satienpong, *An Active Vibration Absorber for Chatter Reduction in Maching*, Department of Mechanical Engineering, The University of Sheffield, 2007.

[9] N.J.M. van Dijk, N. van de Wouw, E.J.J. Doppenberg, H.A.J. Oosterling, and H. Nijmeijer, "Robust Active Chatter Control in the High-Speed Milling Process," *IEEE Transactions on control systems technology,* 2011, vol. 20 no. 4, pp. 901-917.

[10] A. Pesch and J. Sawicki, "Application of Robust Control to Chatter Attenuation for a High-Speed Machining Spindle on Active Magnetic Bearings," in *13th International Symposium on Magnetic Bearings 2012 (ISMB13)*, Arlington, Virginia, USA, Curran, 2013, p. 373.

[11] R. L. Fittro, C. R. Knospe and L. Scott Stephens, "Mu-synthesis Applied to the Compliance Minimization of an Active Magnetic Bearing HSM Spindle's Thrust Axis," *Machining Science and Technology,* vol. 7, no. 1, pp. 19-51, 2003.

[12] K. Gu and S. Niculescu, "Survey on Recent Results in the Stability and Control of Time-Delay Systems," *J. Dyn. Sys., Meas., Control,* vol. 125, no. 2, pp. 158, 2003.

[13] Y. S. Lee, Y.S. Moon, and W. H. Kwon, "Delay-Dependent Robust H-infinity Control for Uncertain Systems with Time-Varying State-delay," Nagoya, 2001.

[14] G. Schweitzer and E. H. Maslen; Eds, *Magnetic Bearings, Theory, Design, and Application to Rotating Machinery*, Berlin Heidelberg: Springer-Verlag, 2009.

[15] S. Boyd, L. El Ghaoui, E. Feron, and V. Balakrishnan, Linear Matrix Inequalities in Systems and Control Theory, Philadephia, PA: SIAM, 1994.

[16] K. Zhou, *Essentials of robust control*, Upper Saddle River, N.J: Prentice Hall, 1998.

[17] G. Genta, *Dynamics of rotating systems*, New York: Springer, 2005.